# TRANSIENT SUBSURFACE FEATURES IN MARS EXPRESS RADAR DATA: AN EXPLANATION BASED ON IONOSPHERIC HOLES

by

Mark Vinton Kane

A thesis submitted in partial fulfillment of
the requirements for the Master of
Science degree in Physics in the
Graduate College of
The University of Iowa

December 2012

Thesis Supervisor: Professor Donald A. Gurnett

Graduate College
The University of Iowa
Iowa City, Iowa

CERTIFICATE OF APPROVAL

-------------------------------------

MASTER'S THESIS

------------------

This is to certify that the Master's thesis of

Mark Vinton Kane

has been approved by the Examining Committee for the thesis requirement for the Master of Science degree in Physics at the December 2012 graduation.

Thesis Committee: ______________________________
Donald A. Gurnett, Thesis Supervisor

______________________________
Steven R. Spangler

______________________________
Kenneth G. Gayley

## ACKNOWLEDGMENTS

I want to thank Dr. Gurnett for introducing me to this problem, and for providing solid guidance and ideas. He has taught me more about what it means to be a scientist than anyone, and for that I'm very much indebted.

I want to thank Don Kirchner for first taking me into the fold of the University of Iowa Plasma Waves Group, and to engineer Willy Robison for his knowledge and comedic interludes. Thanks to David Morgan and J. Douglas Menietti for helping provide the basis of my knowledge of the Martian ionosphere. Special thanks to Doug Menietti and Robert Mutel who independently wrote ray tracing software used in this analysis.

I would also like to thank our support team for their assistance and expertise. Kathy Kurth and Larry Granroth have made working here pleasant and painless. Thanks to Terry Averkamp for providing me with software and data access to the Cain model of the Martian magnetic field, and also to Anne Persoon for proofreading and giving helpful suggestions.

Lastly and most importantly I'd like to thank my loving mother and father, Elaine and Tom, for always offering their support and for being all around great parents, and my two brothers and best friends Jesse and Rudy for their friendship, intelligence, and inspiration.

ABSTRACT

This study was motivated by the discovery of semi-circular subsurface craters, or basins, at multiple locations on Mars by the MARSIS (Mars Advanced Radar for Subsurface and Ionospheric Sounding) radar sounder on board the Mars Express spacecraft. The nature of these subsurface structures was called into question when it was realized that some of the radar observations were not repeatable on subsequent passes over the same region. If they were true geological structures, such as ancient craters buried by dust, one would expect to always see them when the spacecraft passes over these regions. The transient nature of the observations led to the suggestion that these structures were actually of ionospheric origin.

In this paper we will provide evidence, including a proof-of-concept result, that these features are produced by holes in the ionosphere, and not by subsurface structures. We discuss the possibility that the ionospheric holes are caused by an interaction of the ionosphere with local crustal magnetic fields. We introduce the ionospheric model which we used to simulate the MARSIS sounder moving and pulsing radio waves through the Martian ionosphere, and show that the results of ray tracing through this density profile are consistent with data seen in the MARSIS radargrams.

TABLE OF CONTENTS

LIST OF FIGURES

Figure

# CHAPTER I

## INTRODUCTION

The Mars Express spacecraft, which is in orbit around Mars, carries seven primary instruments. One of these instruments is a radar sounder called MARSIS (Mars Advanced Radar for Subsurface and Ionospheric Sounding) that is designed to probe both the subsurface and the ionosphere of Mars [Chicarro et al., 2004]. The main objective of MARSIS is to map the distribution of water, and three secondary objectives are to probe the subsurface geology, to map the surface, and to perform ionospheric sounding. When in subsurface mode the radar will detect subsurface features as far as 5-8 km below the surface [Picardi et al., 2004]. The purpose of this mode is to search for subsurface structures such as water deposits and rock strata, and to map these features to get a better understanding of Mars' geological history. For ease of viewing the data obtained from the subsurface sounding is converted into a radargram, which is a plot of the time delay of the radar echo as a function of time, in order to give a black and white representation of subsurface features. It's analogous to an ultrasound image, except radio waves are used instead of sound waves.

While examining the data, Picardi et al. [2005] found an area in the mid-latitude lowlands of Mars that showed nested parabolic-shaped features in the radargrams. When translated onto a map of Mars these echoes would correspond to a series of concentric rings (Figure A1). The MOLA (Mars Orbiter Laser Altimeter) data, which provides high-resolution images of the surface, from the Mars Global Surveyor spacecraft revealed no above-ground structures in this region that could be causing the radar signature. To explain the parabolic-shaped features, Picardi et al.

[2005] hypothesized that the spacecraft was flying over an underground buried crater (Figure A1) with a nearly flat bottom and a series of concentric reflecting walls giving the signature seen in the radargrams.

The legitimacy of this explanation was thrown into question by Ali Safaeinili (personal communications), and later in a paper by White et al. [2009]. They discovered that the parabolic features appeared in some radargrams and not in others over the same region. This phenomenon was found to occur in many different regions on Mars, and led White et al. [2009] to hypothesize that the unusual signatures were caused by an ionospheric refraction effect.

In this paper we adopt Safaeinili's idea and expand upon it by providing a proof-of-concept argument in favor of refraction by an ionospheric hole as the cause of the parabolic-shaped features. We focus primarily on data obtained while operating in the subsurface mode, and we examine the region with the parabolic-shaped features due to the high level of symmetry of that signature and thus ease of modeling. We provide an ionospheric model, trace rays through it to simulate radar sounding, and compare the results to the radargrams. We also support the model by examining the TEC (total electron content), the magnetic field, and the ASPERA (Analyzer of Space Plasma and Energetic Atoms) plasma data in the regions of interest.

# CHAPTER II

# THE SPACECRAFT

This analysis uses data obtained from the MARSIS (Mars Advanced Radar for Subsurface and Ionosphere Sounding) instrument on the European Space Agency's (ESA) spacecraft Mars Express (Figure A2). MARSIS is a dual-function instrument providing both subsurface radar sounding and ionospheric radar sounding [Picardi et al., 2004].

Mars Express was launched on June 2, 2003 from Baikonur Cosmodrome in Kazakhstan using a Soyuz-FG/Fregat rocket [Chicarro et al. 2004]. Arriving at Mars nearly seven months later, Mars Express entered orbit on December 25, 2003. The spacecraft was put into a highly elliptical orbit with a periapsis altitude of 250 km, an apoapsis altitude of 10,142 km, and an inclination of 86.35$^{o}$. The initial period of the spacecraft was 6 hours and 43 minutes. Because of radar range limitations MARSIS was designed to operate near periapsis at altitudes less than 800 km. Each time Mars Express orbits the planet, MARSIS takes subsurface recordings called passes. On a typical periapsis pass, data is taken for about 26 minutes, usually allowing a mapping of a latitudinal swath of about 100$^{o}$ [Picardi et al., 2004]. Every 11$^{th}$ orbit is over nearly the same region displaced by about 50 km. Thus, adjacent passes can been found after every 11$^{th}$ orbit number.

The spacecraft was developed and built under the direction of the European Space Agency for the purpose of imaging the Martian surface, mapping the mineral composition at the surface, probing the atmosphere, determining the effects of the atmosphere on the surface, understanding the interaction of the atmosphere with the solar wind, and probing the subsurface and ionosphere [Picardi et al., 2004]. The name Mars Express originated from an emphasis by the ESA to accelerate the development and launch of the spacecraft.

The primary source of data for this analysis was radar data obtained by MARSIS. Radar (RAdio Detection And Ranging) is the method of using a transmitter, a receiver, and an antenna to remotely detect a distant object (a target) by transmitting and detecting the returning radio wave pulse after it has bounced off the target. The time delay and Doppler shifts of the returning radio wave pulse can reveal considerable information. For example, the time it takes for the pulse to return to the receiver indicates about how far the reflecting surface is from the transmitter, and the Doppler shift gives information on the angular position of the reflector given the speed of the spacecraft. We take the time of propagation of the radar pulse and combine that knowledge with the speed of the radio wave pulse in the medium we're exploring (e.g., the Martian subsurface) to determine the distance between the transmitter and the reflecting surface (reflector). The usual method of displaying the MARSIS radar data is to make gray-scale plot of the intensity of the returning radar signal as a function of the time delay of the radar echo. This type of plot is called a radargram. A typical radargram is shown in Figure A3. Increasing brightness (white) indicates increasing intensity of the radar echo.

To penetrate through an ionospheric plasma to the surface, the frequency of the radar pulse must be greater than the maximum plasma frequency in the ionosphere. Otherwise it will be reflected. The electron plasma frequency is given by

$$f_{pe} = \frac{\omega_{pe}}{2\pi} = 8980\sqrt{n_e} \text{ Hz} , \qquad (1)$$

where $n_e$ is the plasma number density ($cm^{-3}$) [Gurnett, Bhattacharjee, 2005].

MARSIS is an instrument that is designed to examine ionospheric as well as subsurface structure on Mars using radar. It utilizes a synthetic aperture (Doppler filter) post processing technique, and a dual-frequency transmission to reduce noise/clutter [Picardi et al., 2004] in the radar signals. It transmits at four frequencies: 1.8 MHz, 3.0 MHz, 4.0 MHz, and 5.0 MHz, and is designed to have a radar penetration maximum depth of between 5 and 8 km. The powers of transmission are 1.5 W at 1.8 MHz , and 5.0 W at 3.0, 4.0, and 5.0 MHz. All frequencies have a 1 MHz bandwidth, and transmit for 250 μs. The receive time is 350 μs [Picardi et al, 2004]. The 350 μs receive time seems too short to allow for the radar pulse to reach the ground, much less reach the subsurface, but the 350 μs window is specifically set up so that it starts when the pulse reaches the surface. MARSIS was designed to operate on both the day and night side to allow it maximum global coverage. The plasma frequency on the night side (80+ degrees solar zenith angle (SZA)) is low enough to allow ionospheric penetration by the lower frequency, longer wavelength signals. The lower transmission frequency and lower plasma frequency on the night side make it the ideal place for MARSIS to perform subsurface radar exploration. The high plasma frequencies on the day side tend to reflect or refract the radar radio waves before they get a chance to penetrate to the surface of Mars. Therefore the best results for subsurface sounding are seen on the night side at frequencies of 1.8 and 3.0 MHz [Picardi et al., 2004].

Each radar pulse is transmitted and the return signal is received through a 40 m dipole antenna oriented parallel to the direction of motion. The return signals are received by both the dipole and a second nadir aligned monopole antenna. The monopole, however, has proven to be too noisy to be used so we rely upon the synthetic aperture and dual frequency transmission.

The synthetic aperture is a crucial component for reducing along-track (direction of the spacecraft's trajectory) clutter and sharpening the radar beam, which is otherwise very close to being isotropically transmitted in a far field dipole pattern. It uses Doppler filtering to measure changes in frequency of the radio wave pulse due to the spacecraft motion relative to the surface of Mars and eliminates signals shifted greater than 2.0 Hz. The frequency-shifted components will have reflected components parallel to the direction of motion. The goal of Doppler filtering is to remove those parallel components by limiting the detected signals to a narrow swath that is perpendicular to the direction of the spacecraft's velocity (See Figure A4). This is highly desirable for probing the subsurface because it strongly reduces unwanted reflections from the surface (clutter) along-track. An example of an along-track clutter would be a signal produced by flying toward a mountain, which would appear, due to the larger time delay, as a subsurface feature. Such clutter must be strongly suppressed when attempting to examine signals coming from underground features near nadir. If a feature is not in a plane perpendicular to the velocity of the spacecraft it will be Doppler shifted by an amount

$$\Delta\omega = \omega - \omega' = \vec{\mathbf{k}} \cdot \vec{\mathbf{v}}_{Spacecraft} \qquad (2)$$

[Bellan, 2006]. $\Delta\omega$ greater than 2.0 Hz will be rejected. This translates to an along-track radar beam width between 5-10 km [Picardi et al., 2004], depending upon the altitude of the spacecraft. Note that synthetic Doppler filtering does not eliminate clutter perpendicular to the velocity. The black rectangles in Figure A4 give a qualitative example of the radar footprint after filtering with the synthetic Doppler filter. As noted, the synthetic aperture works for reducing along-track false signals but does not work for off-track clutter perpendicular to the direction of motion. Any clutter in this direction needs to be eliminated by careful examination of the surface geography perpendicular to the direction of travel.

Another method for reducing clutter is the dual frequency broadcast technique. This technique relies on surface clutter power remaining nearly constant for all frequencies, whereas the subsurface power is strongly dependent on frequency. Subtracting the surface signals results in a large reduction in clutter contaminants with the subsurface portion remaining unchanged [Picardi et al., 2004].

In Figure A3 we see clearly the surface of Mars represented as a bright line across the entire picture. The horizontal axis represents position along the spacecraft's trajectory while the vertical axis represents time delay of the reflector. The farther down (vertically) an object appears, the longer it took for the radar pulse to hit and reflect off of it. The brighter a feature appears in a radargram the greater the power of the return signal from that feature.

Neglecting ionospheric effects, the first strong return signal will be that of the surface with a return time of

$$t_0 = 2H / c, \qquad (3)$$

where H is the altitude and c is the speed of light in vacuum. Given the long wavelengths used in subsurface sounding, a significant portion of the radar pulse will be transmitted beyond the surface into the crust. Traveling through the crust, the radio waves enter a different dielectric medium which has a different speed of propagation. The velocity of propagation in the medium is given by,

$$v = c / n = c / \sqrt{\varepsilon_r} \qquad (4)$$

[Reitz, 1979], where $c$ is the speed of light in vacuum, $n$ is the refractive index of the dielectric (here the Martian soil), and $\varepsilon_r$ is the real part of the dielectric constant [Picardi et al., 2004]. The return time for a radio wave penetrating the surface and reflecting off an underground structure is,

$$t = t_0 + 2z_0 / v \qquad (5)$$

where $z_0$ is the depth of the structure. From this equation we can get an estimate of the depth of the target structure [Picardi et al., 2004].

# CHAPTER III

## BURRIED CRATERS

Within the features in the MARSIS radargrams it was found there is a region that shows subsurface nested parabolic-shaped time signatures. We will examine the Mars Orbiter Laser Altimeter data (high definition surface images) to give a picture of the proximity of the orbits from a surface point of view. We will then look at other adjacent orbits to examine the reality of the idea of the signatures originating from subsurface reflectors.

Each time Mars Express orbits Mars, MARSIS takes subsurface radar data. Every 11$^{th}$ orbit is over nearly the same region but displaced in the latitudinal direction by about 50 km. Thus, adjacent passes can been found after every 11$^{th}$ orbit number. We will examine three such adjacent passes on orbits 1881, 1892, and 1903 seen in Figure A5.

Picardi et al. [2005], offered up a geological explanation of the parabolic time signatures (Figures A1 and A6) seen in the radargrams. They hypothesized that buried below the surface was a structure, like an old lake basin or crater. The different parabolic time signatures would each be indicative of a different part of a depression reflecting the radar pulse at different times (Figure A1). Figure A6 illustrates how Picardi et al. thought the buried craters would be situated in the subsurface to give the parabolic signatures in the radargrams.

At first this may seem like a plausible interpretation of the parabolic signatures. However, these features are not always seen in the radargrams. They are transient, appearing and disappearing on adjacent passes (Figure A7). A true geological feature would always be seen in the radargrams on the night side.

The first suspicions about these buried craters were expressed by Safaeinili in personal correspondences with the MARSIS team, and the first publication questioning the buried craters was published by White et al. [2009]. In the White paper the authors showed myriad cases of large underground structures appearing and disappearing in passes over the same geographical regions. The authors then hinted at a possible ionospheric refraction effect which would delay the radar's pulse reflection from the Martian surface enough to give the appearance of underground reflectors in the radargrams. We focus on three specific passes that illustrate this unusual phenomenon. The regions of interest are outlined in Figures A5 and A7 with red rectangles. Mars Express crosses over this night side area at a SZA between 90 and 110 on all of these orbits. There is a lack of both along and off-track structure in Figure A5 around the red rectangles. This confirms that nothing from above ground is causing the parabolic-shaped features we see.

The parabolic-shaped structures can be seen in the red rectangle region of orbits 1892 and 1903 in Figure A7, and these features are magnified in Figure A8. Each of the passes represented in Figure A5 and A7 are displaced from one another by about 50 km off-track. The parabolic structures are about 150 km long in the along-track direction, yet each radargram displays a distinctively different structure. In Figure A7 we included adjacent pass 3819, which occurred at a much later time than the 1881 series, but which was taken in the same region with a nearly identical trajectory as 1903.

Looking at Figure A7 we see that in the pass on orbit 1881 in the red rectangle there is a vague structure but nothing well defined. In the adjacent pass on orbit 3819 there is no structure at all. In the adjacent pass in orbit 1892 there is a clear series of nested parabolic structures. In adjacent pass in orbit 1903 we again see parabolic structures but with different time delays than in 1892, and a hard, flat reflecting structure close to the surface.

These four radargrams illustrate the inconsistencies that can be found in some of the subsurface data. Further examples can be found in White et al. [2009]. The transient nature of these structures leads one to believe that there is a dynamical mechanism likely ionospheric in origin at work causing these inconsistencies.

In the following chapter we propose an ionospheric model and ray trace through it, leading to strikingly similar time delays to those found in the radargrams. In this model the radio waves from the radar will be slowed down in the ionospheric plasma, refract and then reflect off the Martian surface returning to the receiver. The resulting time delay signatures are comparable in shape, magnitude and number to those found in the radargrams.

# CHAPTER IV

# THE MODEL

The goal of our ionospheric model was to introduce a hole with a shape and density profile that would produce time delayed radar returns similar to those seen in the radargrams. We considered two basic choices: a relative plasma density increase such as a higher density lens-like plasmoid, and a relative plasma density decrease such as a hole. The refractive index of plasma, less than one, eliminated the first choice. In that case the refraction of the radar pulse would produce divergent off-nadir rays which after reflection at the surface would not return to the spacecraft. In contrast, as we will show, an ionospheric hole produces convergent off-nadir ray paths which return to the spacecraft with time delays of the same shape as the parabolic time signatures seen in the radargrams. The idea of an ionospheric hole is also supported by the observation of substantial depressions in the total electron content (TEC) in the region where the parabolic features are observed (see Figures A9 and A10). The total electron content is the line integral of the electron density along a vertical line from the spacecraft to the surface, and is given in units of electrons/cm$^2$. Further, there is a depression in the electron energy flux in the ASPERA (Analyzer of Space Plasmas and Energetic Atoms) data, (Figures A9 and A10) (note that ASPERA data is only available for orbit 1903).

The model of the electron density hole that we adopted consists of two main components: a Gaussian vertical distribution and a transverse density variation that represents the hole. A Gaussian provides a good approximation to the electron density near the peak of the Chapman model for planetary ionospheres (Figure A11). The

Chapman model gives the ionospheric density as a function of the ion production rate, solar zenith angle, and altitude [Chapman, 1931]. The transverse part of the model is a hyperbolic tangent term which acts like a gentle step function that gradually turns the density on and off as a function of the transverse distance from the center of the hole. The second feature allows us to make a hole in the ionosphere while retaining a Gaussian style profile. The density model is given by,

$$n_e(x,z) = n_0 H(z) \cdot T(x) \tag{6}$$

$$H(z) = \exp[-(z-h_0)^2 / 2\sigma^2] \tag{7}$$

$$T(x) = 1/2(1+\tanh[(\cos\ \Psi)\cdot(|x|-x_0)/w]) \tag{8}$$

Where *H(z)* gives the vertical height dependence, *T(x)* gives the transverse dependence, $n_0$ is the maximum plasma density, *z* is the altitude, $h_0$ is the altitude of the peak electron density, $\sigma$ gives us the vertical width of the Gaussian function, *x* is the horizontal distance, $x_0$ is the transverse size of the hole, and *w* controls the steepness of the step function. The $\Psi$ term in the cosine nested in the hyperbolic tangent allows us to gradually turn the hole on and off again (see Figures A4 and A12(a,b,c)) simulating the spacecraft flying over the hole. At $\Psi$ = -90$^o$ we are at the beginning of the hole (Figure A4), at $\Psi$ = 0.0$^o$ we are at the middle of the hole, and at $\Psi$ = 90$^o$ we have reached the end of the hole. The parameters used in the model were, $n_0$ = 1.0X10$^5$, $h_0$ = 130.0 km, $\sigma$ = 35.5, $x_0$ = 75.0 km, and *w* = 30, giving a maximum plasma frequency of 2.8 MHz, low enough to give substantial refractions of the radar pulse. Note that we use Cartesian coordinates due to the large Martian radial distance compared with the size of our model.

Figure A4 shows a top down view of Mars Express as it flies over the hole. Each of the black lines represents a transverse swath that is being sampled by the synthetic aperture mentioned in Chapter 2. Notice that the along-track radar beam width is small compared with the cross-track width due to the synthetic aperture.

Figure A12 shows the view of Mars Express in the along-track direction, into the paper. It starts with no hole, A12.a which corresponds to pulse 1 at $\Psi = -90^o$ of Figure A4. We then move through the hole, A12.b, corresponding to pulse 2 at $\Psi = -45.0^o$ in Figure A4. Finally we reach the center of the hole, A12.c, corresponding to pulse 3 at $\Psi = 0.0^o$ in Figure A4. After we traverse the middle of the hole, the echo pattern is same as before, just mirrored.

# CHAPTER V

## RAY TRACING AND RESULTS

To perform the ray path calculations we had the good fortune of having access to two independently written ray tracing software programs. The software for the two programs were written by Doug Menietti and Robert Mutel, both of the University of Iowa. Menietti's program was written in Fortran while Mutel's was written in Python. Both of these programs were based on the Haselgrove system of equations which are based on Hamilton’s principle in geometric optics as applied to radio waves propagating in a plasma [Haselgrove, 1955]. The programs allow one to emit a radio wave through an arbitrary plasma density profile geometry and see how the radio waves are refracted by the plasma. It would be comparable to turning on a light bulb and computationally knowing which parts of the room were well illuminated, and which ones not. Note that although we only show a discrete set of ray paths, all angles below the spacecraft were assessed.

Adjusting the parameters of the hole, namely its density and shape allowed us to come up with a model with a density comparable to that found in the Martian ionosphere on the early night side as provided by Chapman (Figure A11). The wave normal angle must be adjusted at the modeled surface of Mars to give an equal angle reflection. This allows the ray to bounce upon hitting the surface of Mars to complete a return to the spacecraft.

In Figures A13.a, A13.b, and A13.c the spacecraft is flying into the page. In Figure A13.a there is no ionospheric hole. The ray paths go through a Gaussian shaped ionosphere, refract, bounce off the surface, reenter the ionosphere, and do not return to the spacecraft. In Figure A13.b the spacecraft is now over a portion of the hole. The ray paths are now taking 5 unique round-trip paths from and to the spacecraft. In Figure A13.c the spacecraft is at the widest portion of the hole and the 5 unique round-trip paths are now the most pronounced.

Performing ray tracing (Figures A13(a,b,c)) yields time delay results of the same order of magnitude as those found in the radargrams. More importantly, the delay patterns are the same nested parabolic shape as seen in the radargrams. The time delays are represented in Figure A14 and compared with those seen in radargrams 1892 and 1903 (Figures A15 and A16). One can imagine the hole starting at around -75 km in Figure A14, with the center being at 0 km, and then progressing with the hole ending at around 75 km. When we say that the hole ends and begins we use this terminology loosely. The nature of the model is such that it takes values over all $x$ and $z$, so there is never an area that is completely void of plasma, just areas that have relatively greater or lesser densities.

From the ray tracing we get exactly five distinct ray paths that return to the spacecraft. This is noteworthy given that in the adjacent passes in orbits 1892, 1903 we have five distinctive echoes. It should be noted that the spacecraft must be displaced from the center of the hole to achieve five distinct ray paths. If the spacecraft is placed in the center of the hole we achieve only three distinct ray paths. It seems reasonable to assume that if there is a hole, it is more likely that the spacecraft will be traveling off center than directly over the center.

# CHAPTER VI

# DISCUSSION

Understanding inconsistencies in the interpretations of the radargrams, interpreting available data, and reproducing the radargrams with our model has led us to the conclusion that there are ionospheric holes in the region we focused on in this study. In our ray tracing results the number of the time delays are consistent with the radargrams and the shape of the modeled return paths is similar to the nested parabolic-shaped features seen in the radargrams. The time delays while not exact are of the same order of magnitude as those observed, i.e. within a few tenths of a millisecond. We think this discrepancy can be rectified by decreasing the plasma density and adjusting the shape of the ionospheric model.

Other interesting features in the regions of the 1892 and 1903 parabolic features are the local crustal magnetic field [Cain, 2003], total electron content (TEC), and ASPERA (Analyzer of Space Plasmas and Energetic Atoms) data, (Figures A9 and A10) (note that ASPERA data is only available for orbit 1903, but not 1892).

In Figures A9 and A10, the red rectangle indicates the same regions. In Figure A9 we see the nested parabolic features in the radargram. We also see a clear and significant drop in the TEC. Of note is a magnetic structure which appears upstream (lower SZA) from the hole. We do not have ASPERA data for this pass.

In Figure A10 we see similar nested parabolic features. Again there is a drop in the TEC, and a similar magnetic structure to that seen in Figure A9, the pass of orbit 1892. For this pass we also have ASPERA data which show a clear drop in electron energy flux.

The radial magnetic fields in this region are peaked before the parabolic features and close to zero in the center of the parabolic features. The theta component of the magnetic field is peaked in the center of the parabolic features. The SZA in this region is 90-110, meaning that the spacecraft is on the early night side. This is of interest because it gives the crustal magnetic field an opportunity to connect with the downstream magnetic field of the solar wind.

It is clear that in this region we have a transient hole in the ionospheric plasma. Our ray tracing results have confirmed the feasibility of our hole model which in turn agrees with the data in the region. Going beyond our model these ideas can be extended and applied to more regions with more complicated magnetic fields and ionospheres to test for ionospheric distortions in the radargrams and thus reduce noise.

The question remains as to what is causing the holes. It should be noted that the ion production rate on the dayside of Mars is much higher than on the night side, and that the higher density day side plasma has a tendency to waft over to the early night side. In the frame of reference of the crustal magnetic field the ionospheric plasma will have a velocity due to the planet's rotation, and plasma with components of the velocity perpendicular to the magnetic field will experience a Lorentz force. This force may cause plasma to be excluded from the region resulting in a hole. A second possibility is that since we are dealing with events on the early night side a sufficiently thermally energetic day side plasma wafting over to the early night side and a crustal magnetic field with open field lines connecting to the solar wind could allow a plasmoid to escape the ionosphere along field lines in a way similar to that of a coronal mass ejection leaving a hole in its place. The downstream nature of the holes from the magnetic fields, seen in Figures A9 and A10, may point toward this conclusion.

# APPENDIX

## FIGURES

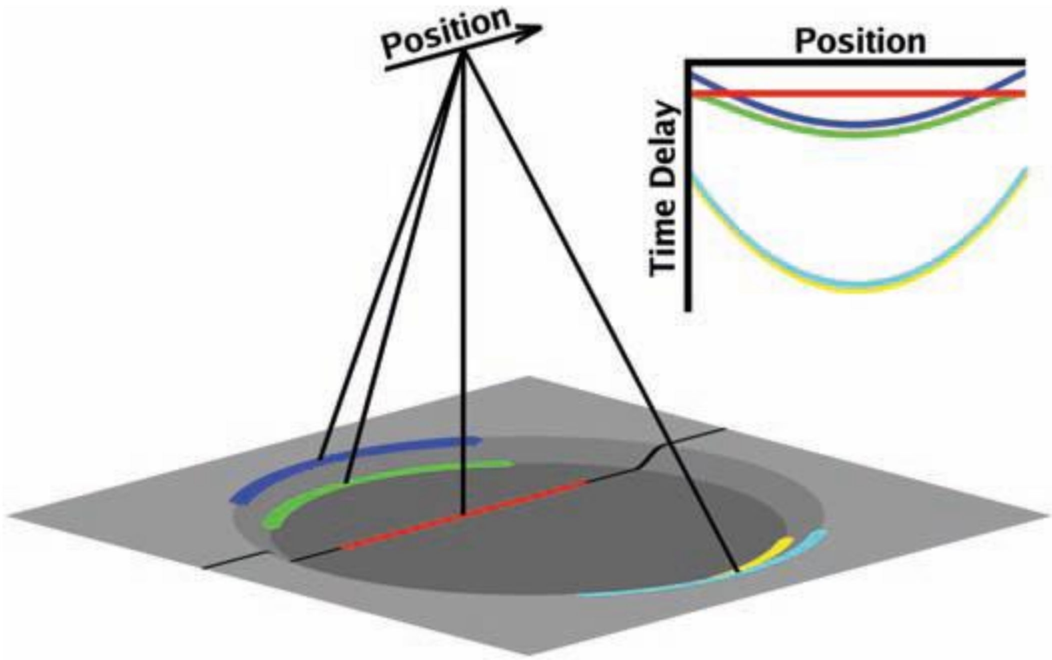


Figure A1. A geographical explanation of the parabolic features seen in the radargrams [Picardi et al., 2005]. The basin is buried. The edges of the basin give a parabolic signature in the radargrams.

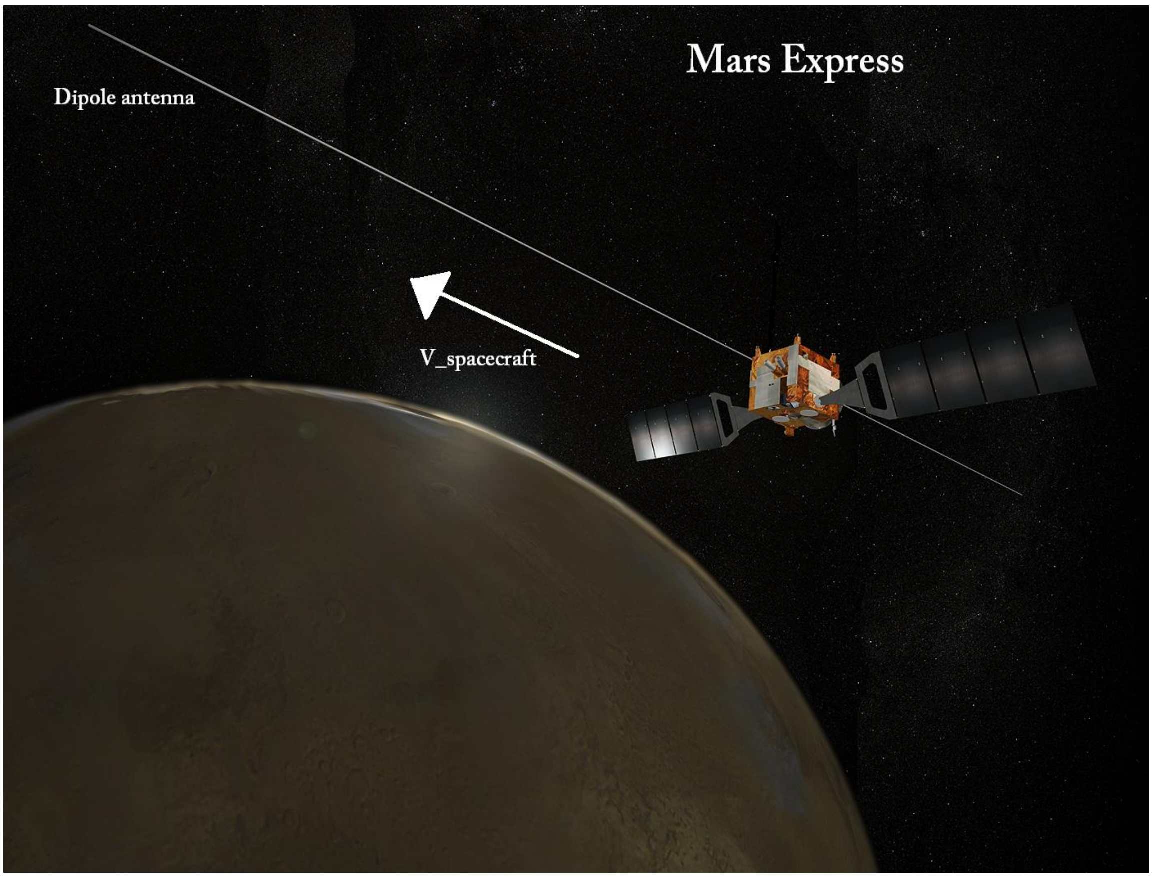


Figure A2. Mars Express. Note that it moves in a direction parallel to the axis of the dipole antenna (picture courtesy of NASA).

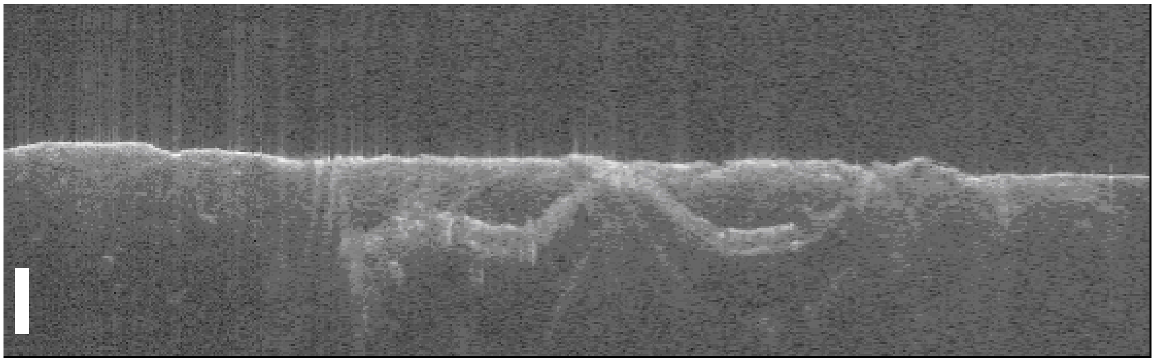

Figure A3. A Martian radargram. The bright line in the middle represents the surface, while the dipping structures below the surface represent some sort of structure. The white vertical bar represents 25μs travel time.

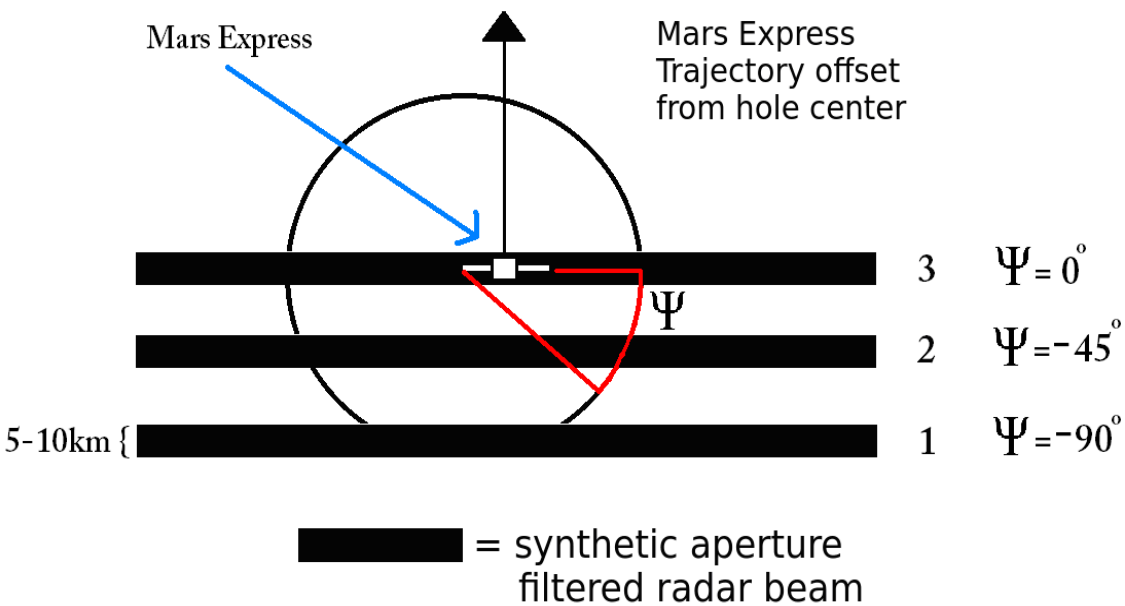


Figure A4. Top down view of Mars Express flying over an ionospheric hole. Blue arrow points to the spacecraft. The red arc gives the psi parameter. Black bars (swaths) illustrate three separate radar pulses narrowed along-track using synthetic Doppler filtering. In the model the swaths are 5-10 km wide along-track. Their along-track width here is exaggerated. The hole is 150 km in diameter.

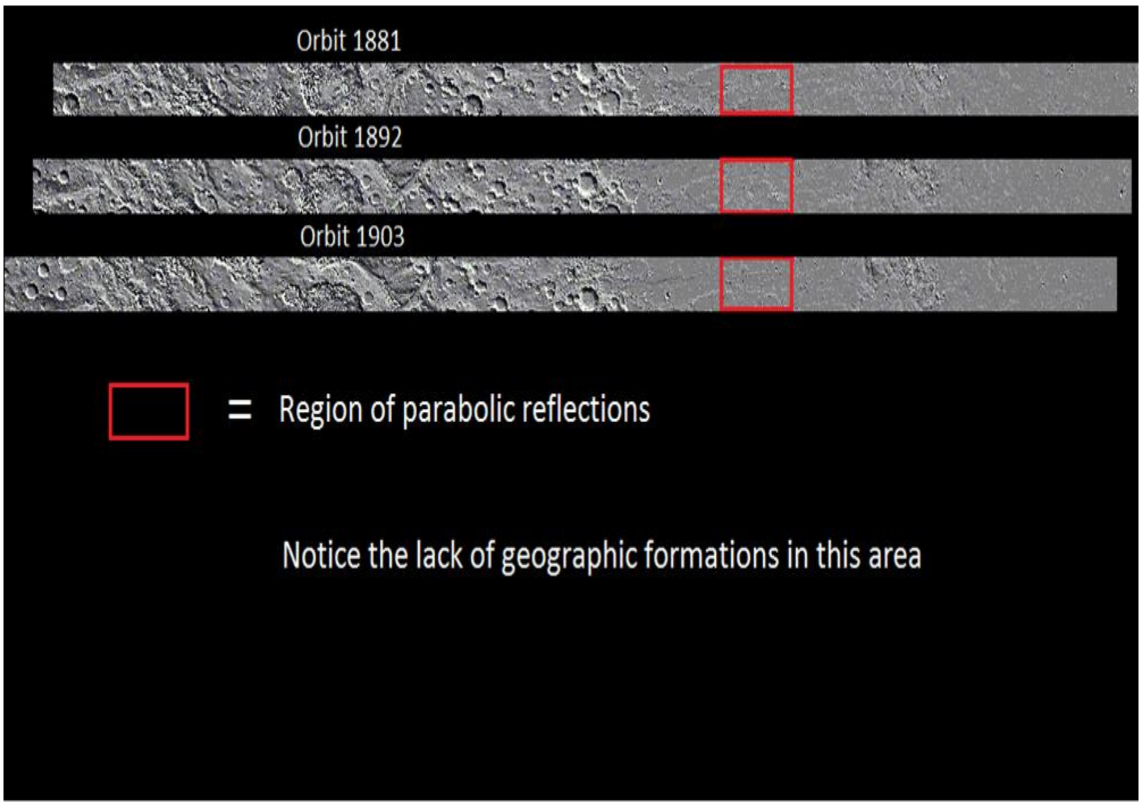


Figure A5. Comparison of three adjacent passes on orbits 1881, 1892, 1903, as viewed from the top. Notice the crater patterns in the center of pictures that shows alignment of the orbits. The orbits are offset from one another by nearly 50 km. Red rectangles highlight the location of the subsurface parabolic structures

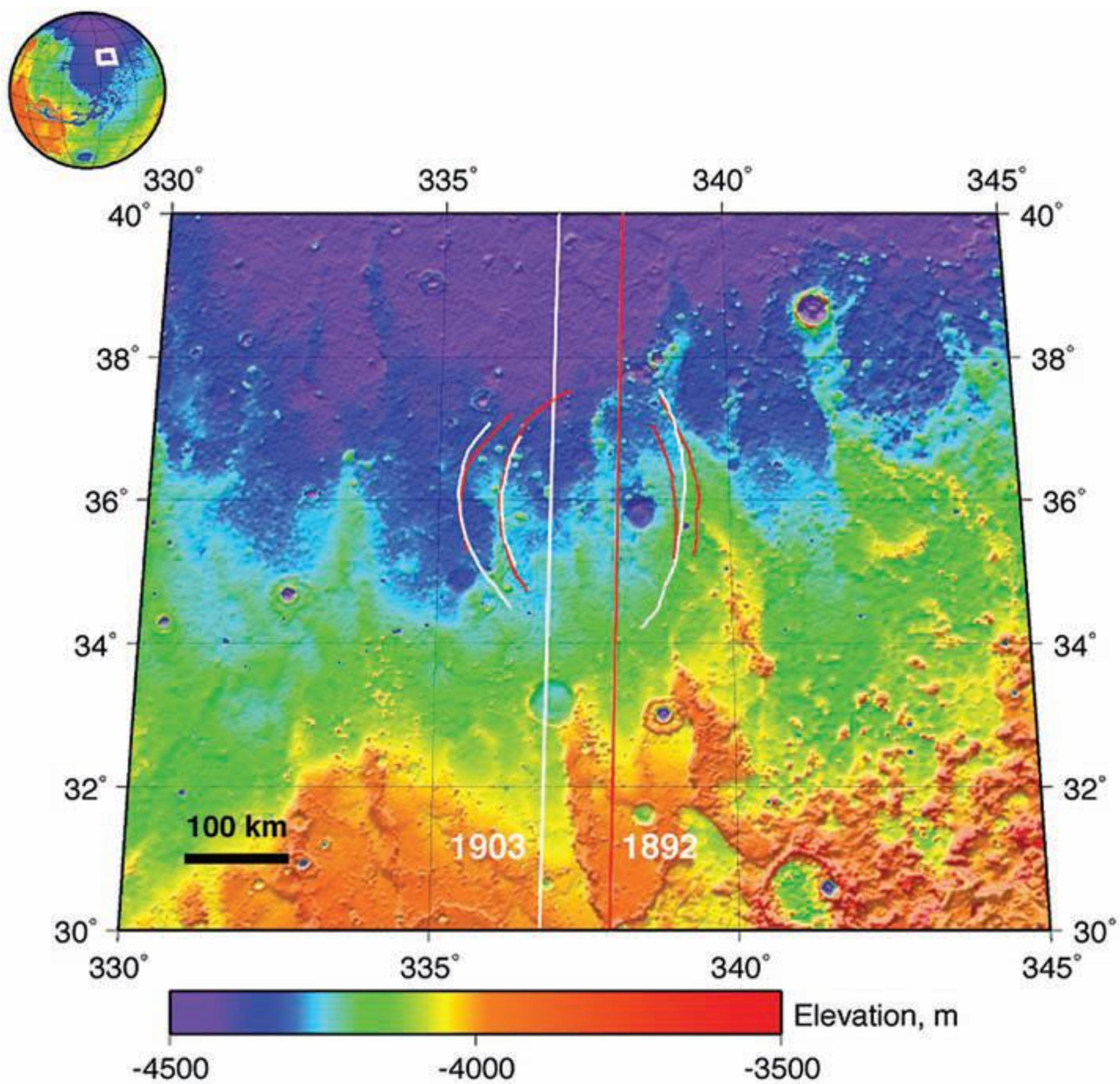


Figure A6. Locations of the circular structures as predicted by Picardi et al. [2005].

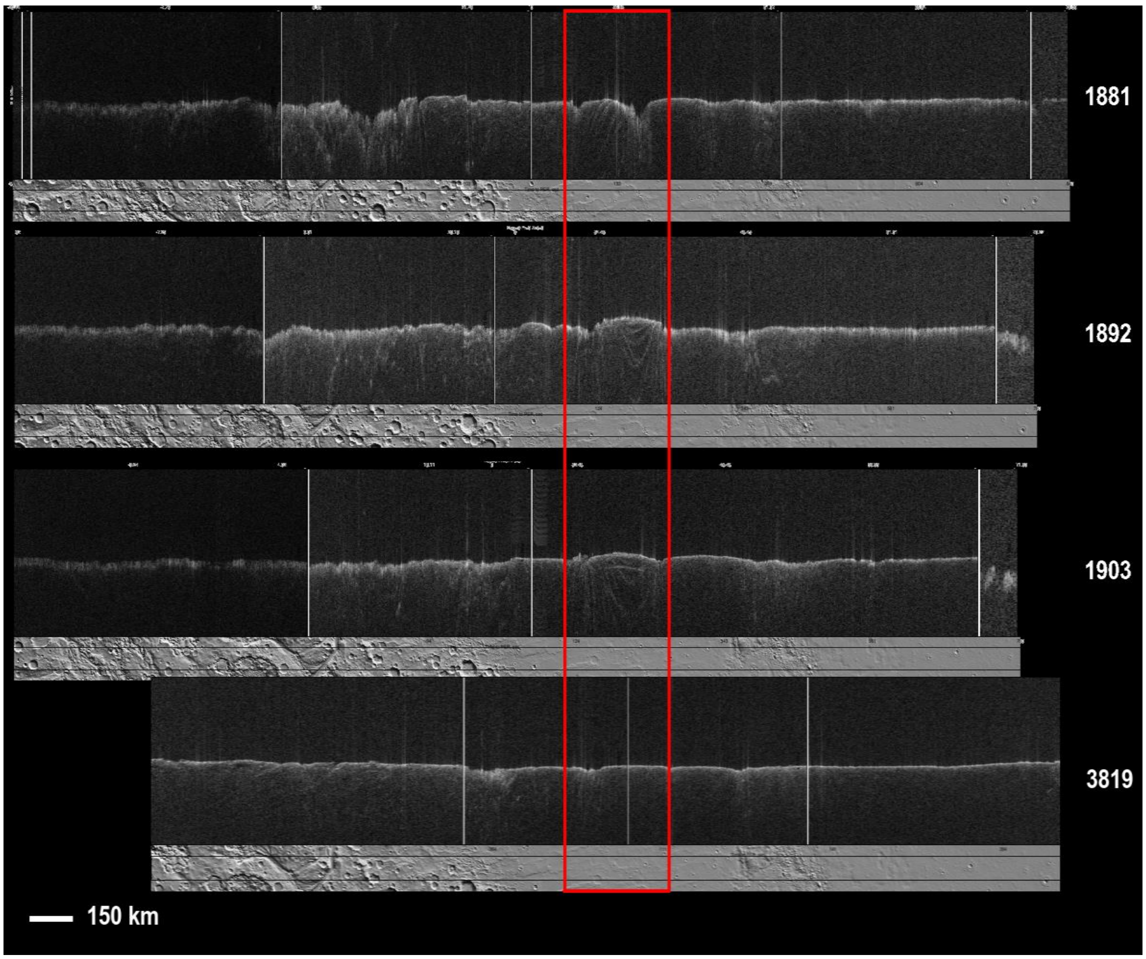


Figure A7.  Radargrams of adjacent passes.

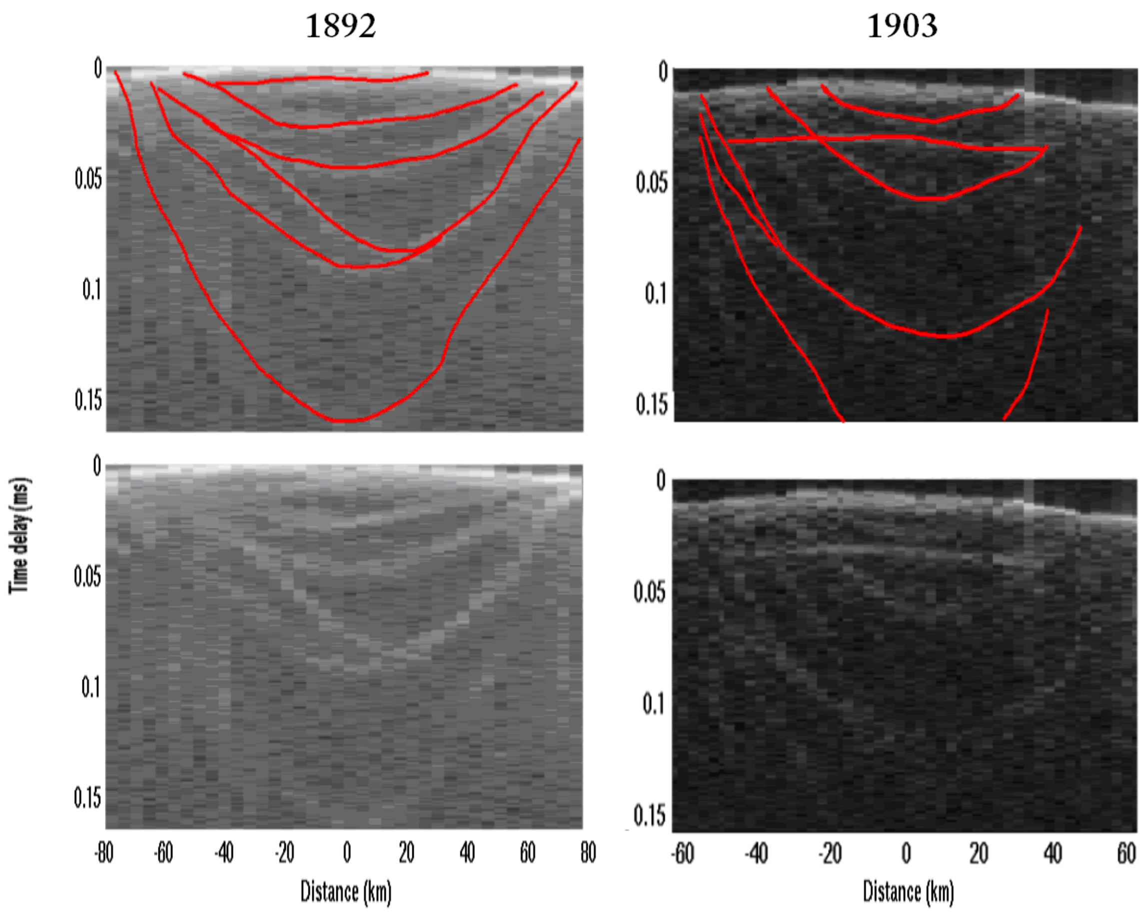


Figure A8.  Zoomed in view of the parabolic structures of adjacent passes in orbits 1892 and 1903.

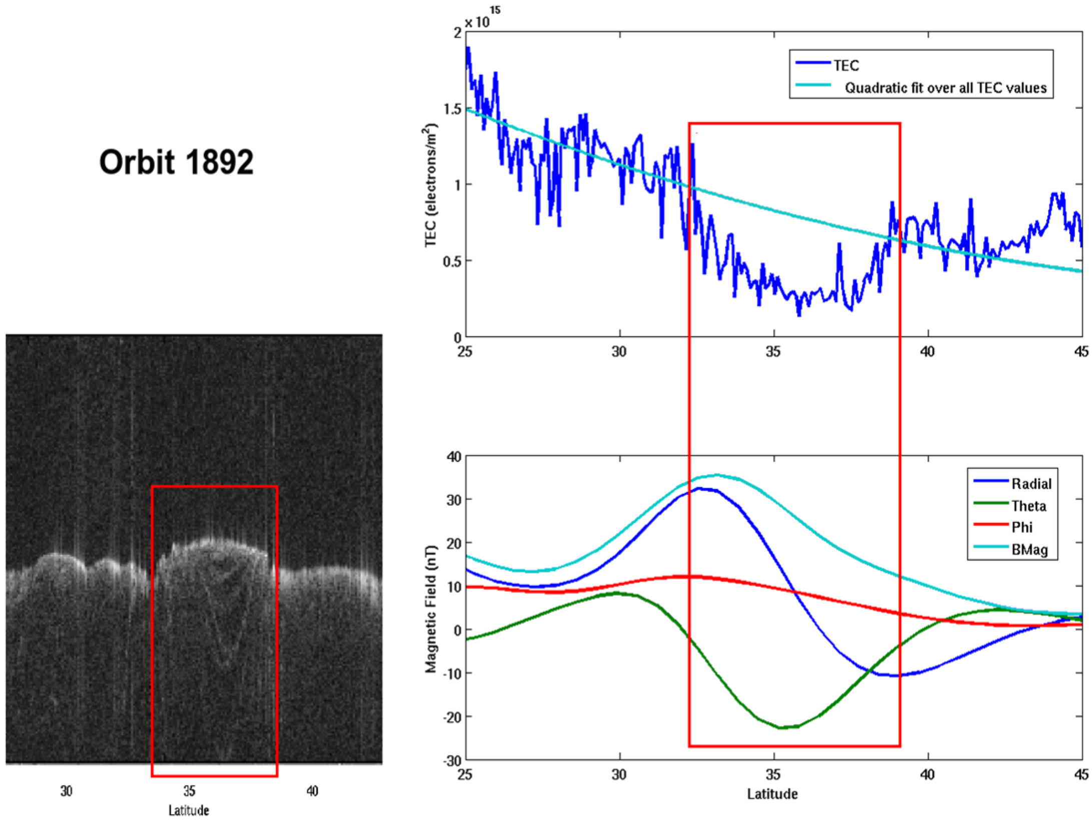


Figure A9. Comparison of TEC, radargram, and magnetic field data of the pass in orbit 1892.

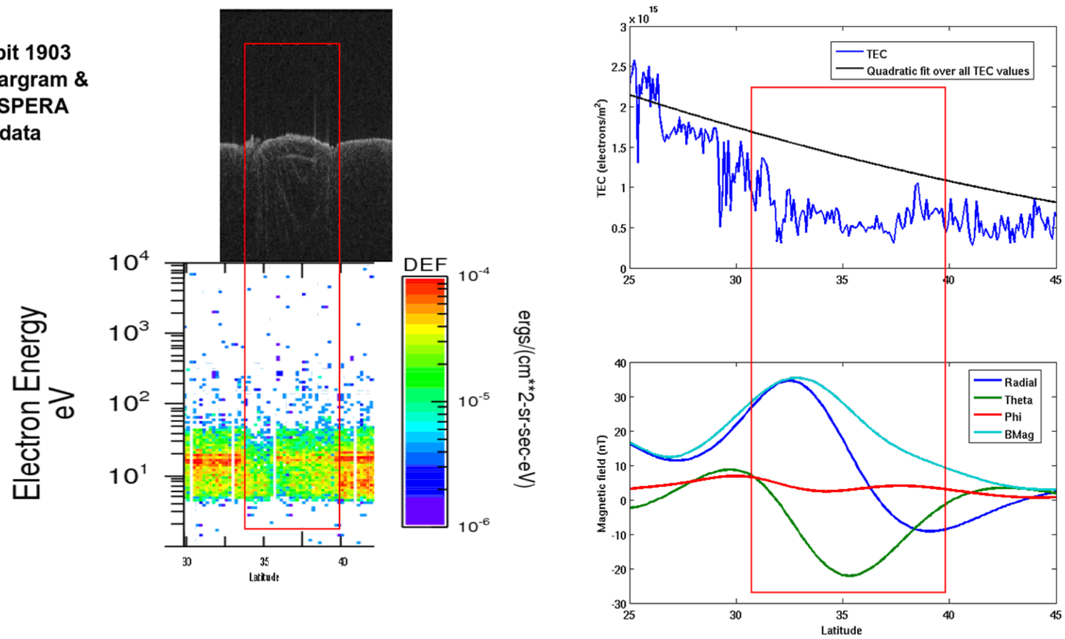


Figure A10. Comparison of radargram, TEC, ASPERA, and magnetic field data in the pass in orbit 1903.

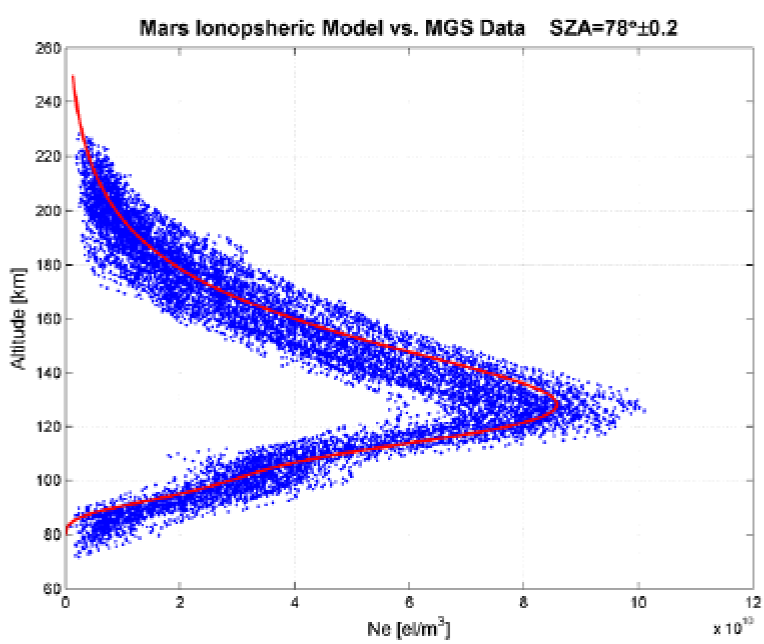


Figure A11. The Chapman ionospheric model (red) with Mars Global Surveyor (MGS) radio occultation density profile data (blue) plotted over it [Pi et al., 2008].

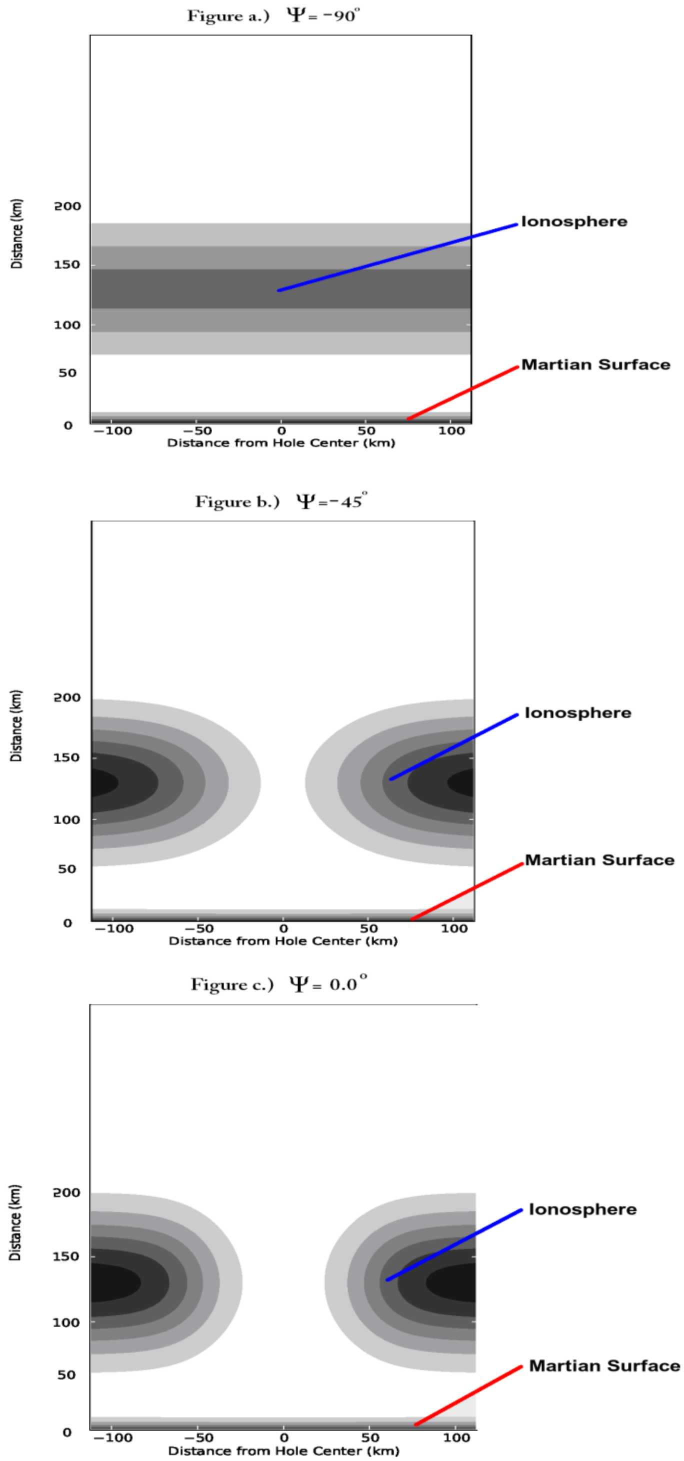


Figures A12(a,b,c). Cutaways of the model ionosphere. Top down view can be seen in Figure A4. A12.a.) No hole yet. A12.b.) ¼ of the way over the hole. A12.c.) Directly in the middle of the hole with the widest opening. This is also where we see the longest time delays from the five ray paths.

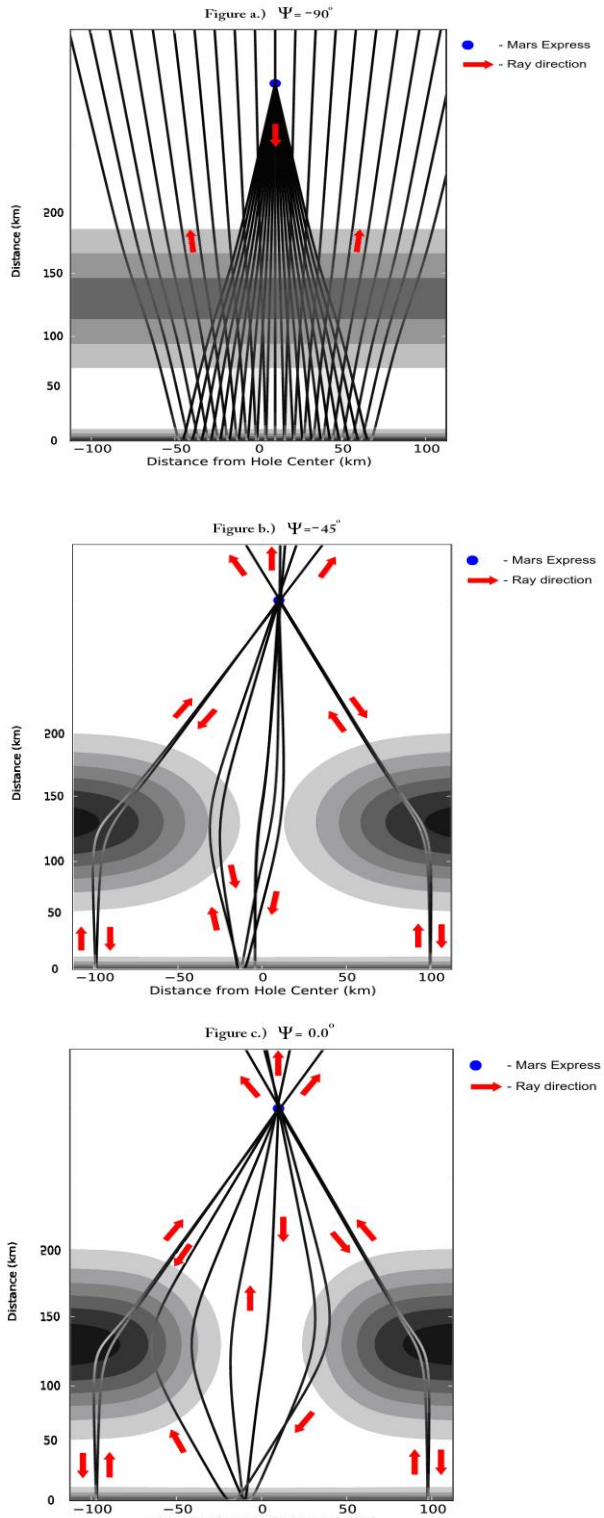


Figure A13(a,b,c). The same as Figures A12(a,b,c), but with Mars Express ray tracing through the ionosphere. Note that all angles were tested for a return path, but only the five shown in A13.b and A13.c produce a return.

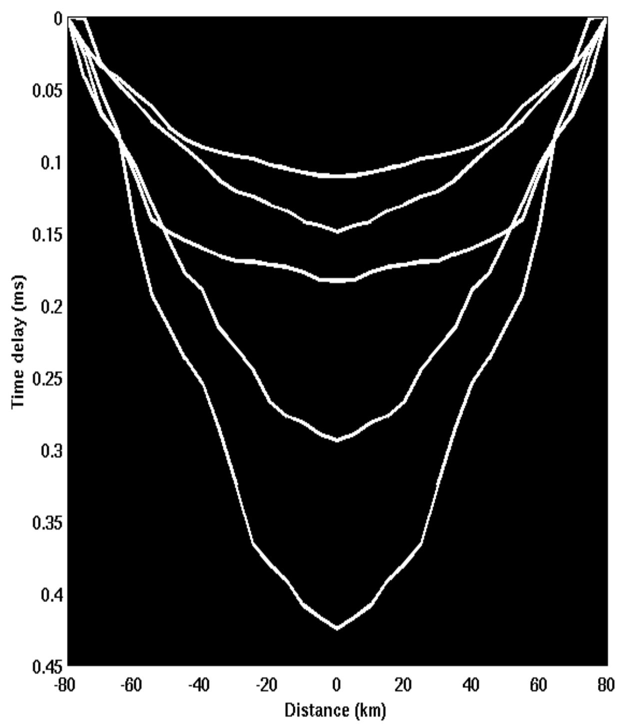


Figure A14. Ray tracing results.

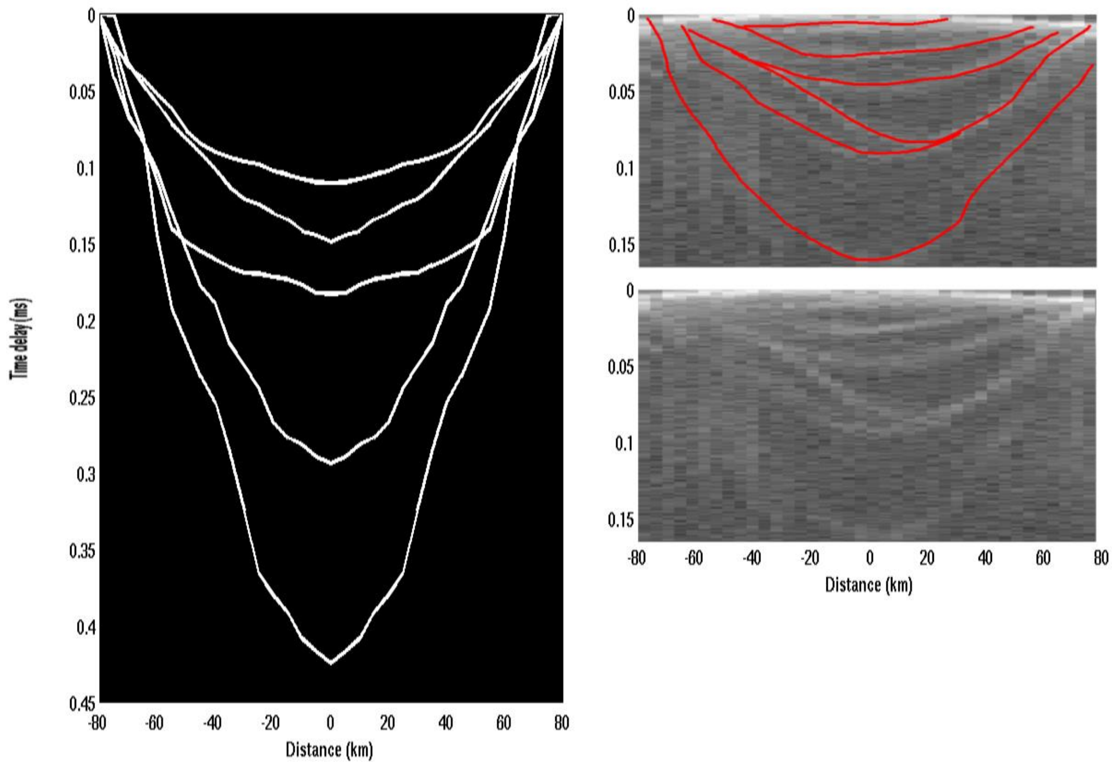


Figure A15. Comparison of the ray tracing results with the pass in orbit 1892.

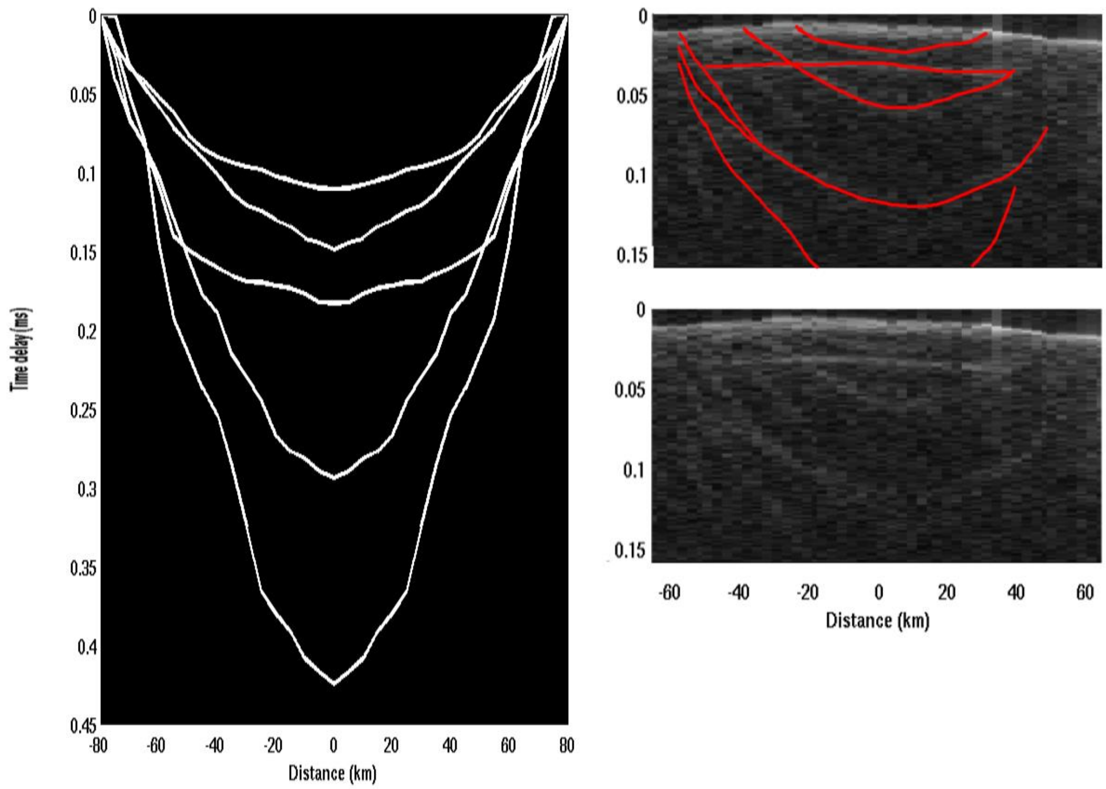


Figure A16. Comparison of the ray tracing results with the pass in orbit 1903.

# REFERENCES

Bellan, P., 2006, *Fundamentals of Plasma Physics*, Cambridge University Press

Cain, J. C., B. B. Ferguson, and D. Mozzoni, 2003, *An n = 90 internal potential function of the Martian crustal magnetic field*, J. Geophys. Res., 108(E2), 5008

Chapman, S., *The absorption and dissociative or ionizing effect of monochromatic radiation in an atmosphere on a rotating earth*, Proc. Phys. Soc.(London), 43, 26-45, 1931

Chicarro, A., Martin, P., Traunter, R., 2004, *Mars Express: A European Mission to the Red Planet*, SP-1240, pp. 3-16, European Space Agency Publication Division, Noordwijk, Nederlands

Gurnett, D. A. and A. Bhattacharjee, 2005, *Introduction to Plasma Physics*, Cambridge
Univ. Press, Cambridge, UK, 11.

Haselgrove, J.: 1955, *Ray Theory and a New Method for Ray Tracing*, London Physical Society Report of Conference on the Physics of the Ionosphere. pp. 355–364.

Pi, X., Edwards, C., Hajj, G.., Ao, C., Romans, L., Callas, J., Mannucci, A., Asmar, S., Kahan, D., *A Chapman-Layers Model for Mars*, 2008, JPL Publication

Picardi, G., Biccari, D., Seu, R., Plaut, J., Johnson, W.T.K., Jordan, R.L., Safaeinili, A., Gurnett, D.A., Huff, R., Orosei, R., Bombaci, O., Calabrese, D., & Zampolini, 2004, E., MARSIS: Mars Advanced Radar for Subsurface and Ionosphere Sounding, *Mars Express: A European Mission to the Red Planet*, ed. by A. Wilson, ESA Report SP-1240, European Space Agency Publications Division, ESTEC, Noordwijk, The Netherlands, Paris, France, pp. 51-69

Picardi, G., Plaut, J., Biccari, D., Bombaci, O., Calabrese, D., Cartacci, M., Cicchetti, A., Clifford, S., Edenhofer, P., Farrell, W., Federico,C., Frigeri, A., Gurnett, D.A., Hagfors, T., Heggy, E., Herique, A., Huff, R.L., Ivanov, A., Johnson, W., Jordan, R., Kirchner, D.L., Kofman, W., Leuschen, C.J., Nielsen, E., Orosei, R., Pettinelli, E., Phillips, R.J., Plettemeier, D., Safaeinili, A., Seu, R., Stofan, E.R., Vannaroni, G., Watters, T.R., Zampolini, E., 2005, *Radar Soundings of the Subsurface of Mars*, Science, 310, 1925

Reitz, J.R., Milford, F.J, Christy, R.W., 1979, *Foundations of Electromagnetic Theory*, Addison-Wesley Publishing

White, O.L., A. Safaeinili, J.J. Plaut, E.R. Stofan, S.M. Clifford, W.M. Farrell, E. Heggy, G. Picardi, 2009, *MARSIS Radar Sounder Observations in the Vicinity of Ma'adim Vallis, Mars*, Icarus, vol 201, issue 2, pp. 460-473